

Tsunami effects on the Z component of the geomagnetic field

Klausner V.^{a,b}, Domingues M. O.^d, Mendes O.^b, Papa A. R. R.^{a,c}

^aNational Observatory - ON 20921-400, RJ, Brazil

^bDGE/CEA/National Institute for Space Research - INPE 12227-010 São José dos Campos, SP, Brazil

^cRio de Janeiro State University - UERJ, RJ, Brazil

^dLAC/CTE/National Institute for Space Research - INPE 12227-010 São José dos Campos, SP, Brazil

Abstract

The vertical component (Z) of the geomagnetic field observed by ground-based observatories of the INTERMAGNET network has been used to analyze the effects of the movement of electrically conducting sea water through the geomagnetic field due to a propagation of a tsunami. The purpose of this work is to study the geomagnetic variations induced by the tsunamis occurred at 26 December, 2004, 27 February, 2010 and 11 March, 2011. For each case study, we selected four magnetic stations belonging to the INTERMAGNET programme that were influenced or more direct affected by the tsunami. To detect these disturbances in the geomagnetic data, the discrete wavelet technique have been used in four levels of decomposition. We were able to detect the localized behavior of the geomagnetic variations induced by the movement of electrically conducting sea-water through the geomagnetic field, *i. e.*, the identification of transients related to the tsunamis. As well, using the minutely magnetogram data, it was able to localize the initial phase and time of the tsunami maximum height. The first interpretation of the results suggests that discrete wavelet transform can be used to characterize the tsunami effects on the geomagnetic field, but need further study.

Keywords: geomagnetic storm, magnetogram, wavelet, tsunami

1. Introduction

In the treatise “De Magnete” as early as 1600, the english researcher Gilbert showed the predominately dipolar character of the terrestrial magnetic field. Next in the early nineteen century, other english researcher Gauss improved the magnetic field observation techniques and introduced the spherical harmonic method for geomagnetic field analysis. Based on a called “Spherical Harmonic Analysis”, a mathematical method was developed to separate the external and the internal contributions to the surface field by a unique global analysis of the Earth’s main field (see Campbell, 1997, and references therein).

The geomagnetic field is described as a complicated function of space and time. Ground based magnetic measurements show a repetitive diurnal variation on geomagnetically quiet days. But there is a great variety of irregular variations that occur from time to time, the “disturbance fields”. Periods of great disturbance are called, by analogy with the weather, “magnetic storms” (Parkinson, 1983).

Some evidence of the influence of oceanic tides on the magnetic daily variation has been obtained by Larsen and Cox (1966). They found small semidiurnal variations of the Z component at a coastal site (Cambria, California) and at two island stations (Honolulu and San Miguel) that

Preprint submitted to J. Atm. Sol-Ter. Phys.,

24 August 2011

17 could not be explained by the atmospheric tidal theory. They suggested that these variations
 18 must be due predominantly to oceanic tides. It is important to mention here that the conductivity
 19 of the ocean does not vary significantly with time, unlike the ionospheric conductivity. As a
 20 consequence, the seasonal variation of the oceanic contribution is expected to be smaller than the
 21 ionospheric contribution (Cueto et al., 2003).

22 Manoj et al. (2011) observed the geomagnetic contributions due to the moderate tsunami
 23 in the Pacific ocean provoked by the Chilean earthquake of 8.8 in magnitude at three different
 24 magnetic stations (PPT, HUA and IPM). Their observations presented a variation of 1 nT in
 25 the vertical component of the magnetic field (Z) during the time of the tsunami effects. Move-
 26 ment of electrically conducting sea-water through the geomagnetic field generates an electromo-
 27 tive force that induces electric fields, currents and secondary magnetic fields. In other words,
 28 tsunamis can produce perturbations in the Earth's magnetic field by electro-magnetic induction
 29 (see Manoj et al., 2011, and references therein).

30 In this work, we focused on the survey of geomagnetic variations induced by some selected
 31 tsunamis: one of 26 December 2004, other of 27 February 2010 and another of 11 March, 2011.
 32 As the wavelet transforms had turned out to be a very useful tool in atmospheric signal analysis
 33 (see Domingues et al., 2005, and references therein), the discrete wavelet technique has been
 34 selected and used with four levels of decomposition in order to detect the small singularities
 35 in the geomagnetic data. For a good revision on the application of discrete wavelet on Space
 36 Weather Research, Domingues et al. (2005), Mendes et al. (2005) and Mendes da Costa et al.
 37 (2011) can be consulted. Thus, this work aims to verify the use of the wavelet technique as a way
 38 to identify the effects related to tsunamis on the geomagnetic field components, particularly the
 39 Z-component. The contents are composed by: in Section 2, the presentation of the geomagnetic
 40 disturbance mechanism related to the tsunami effects; in Section 3, applied the methodology;
 41 in Section 4, the data; in Section 5, the results achieved by the analysis; and in Section 6, the
 42 conclusions of our work.

43 2. Geomagnetic disturbance mechanism

44 Faraday originally predicted that ocean waves could induce electrical fields, which are also
 45 called by "motional induction". The induction mechanism process consists of the flow of the
 46 ocean water, as an electrically conducting fluid, through the Earth's main magnetic field. The
 47 salts dissolved in the sea water are made of ions that can be deflected by the Lorentz force which
 48 acts in a perpendicular direction both to the velocity and magnetic field vectors (Tyler et al.,
 49 2003; Manoj et al., 2006). As consequence of the motion of sea water with velocity \vec{V} across the
 50 geomagnetic field \vec{B} , a conduction current \vec{J} is produced expressed by:

$$\vec{J} = \sigma (\vec{E} + \vec{V} \times \vec{B}), \quad (1)$$

51 where σ is the electrical conductivity, \vec{E} is the stationary electric field and $\vec{V} \times \vec{B}$ is the induced
 52 electric field. Discarding any displacement current, the Ampere's law is used to determine an
 53 induced magnetic field \vec{b} given by:

$$\vec{\nabla} \times \vec{b} = \mu_0 \vec{J}, \quad (2)$$

54 where $\mu_o = 4\pi 10^{-7}$ henry/m. It is known that electric and magnetic fields are related by
 55 Faraday's law given by:

$$\vec{\nabla} \times \vec{E} = \frac{\partial \vec{b}}{\partial t}. \quad (3)$$

56 Applying the same mathematical development used by Podney (1975), the velocity field
 57 present in the problem can be described as a curl of a vector stream function $\vec{\Psi}$ (the stream
 58 understood as the flow of the ocean water), *i.e.*:

$$\vec{V} = \vec{\nabla} \times \vec{\Psi}. \quad (4)$$

59 In analogy, the induced magnetic field can be expressed by a vector potential \vec{A} , given by:

$$\vec{b} = \vec{\nabla} \times \vec{A}. \quad (5)$$

60 Thus the relation between the vector stream function $\vec{\Psi}$ and the geomagnetic field \vec{B} as a function
 61 of the vector potential \vec{A} can be established as:

$$\nabla^2 \vec{A} - \mu_o \sigma \frac{\partial \vec{A}}{\partial t} = -\mu_o \sigma \vec{\nabla} \times (\vec{\Psi} \times \vec{B}). \quad (6)$$

62 In a short description, the induced magnetic field generated by the ocean can be classified by
 63 two components: toroidal and poloidal. The toroidal component is generated by the electrical
 64 currents closing in the vertical plane and can reach up to 100 nT but is confined to the ocean and
 65 the upper crust. The poloidal component is much weaker, between 1 and 10 nT, and arises from
 66 the electrical currents closing in the horizontal plane, however it can reach outside of the ocean
 67 to remote lands and satellite locations (see Tyler et al., 2003; Manoj et al., 2006, and references
 68 therein).

69 The sea water is subject to two kinds of geomagnetic fluctuations: periodic (lunar and solar
 70 variations) and transient disturbances (geomagnetic storms), as discussed by Longuet -Higgins et al.
 71 (1954). Also, the ocean flow can be occasionally disturbed by tsunamis that can increase the
 72 ocean wave speed for few centimeters per second and that affects the entire water column. Con-
 73 sequently, as demonstrated before, to increase the ocean flow will also increase the magnetic
 74 induced field.

75 Considering quiet conditions, Tyler et al. (1999) discussed that the major difficulty to deter-
 76 mine the magnetic ocean generated signals are the weak values compared to the signals from
 77 other sources. This is the reason to take advantage of some analysis features of the wavelet
 78 technique.

79 3. Discrete Wavelet Transform (DWT) methodology

80 The wavelet transforms were better and broadly formalized thanks to mathematicians, physi-
 81 cist, and engineers efforts (e.g., Morlet, 1983). In the domain of geophysics applications, the
 82 main characteristic of the wavelet technique is the introduction of time-frequency decomposition
 83 (e.g., Domingues et al., 2005; Mendes et al., 2005; Mendes da Costa et al., 2011). In the 1990s
 84 several important ideas and applications concerning wavelet were developed (e.g., Daubechies,
 85 1992; Chui, 1992a,b, 1994).

86 The wavelet analysis could show that the larger amplitudes of the wavelet coefficients are lo-
 87 cally associated with abrupt signal changes. In recent work (Domingues et al., 2005; Mendes et al.,
 88 2005; Mendes da Costa et al., 2011), a method for the detection of the transition region and the
 89 exact location of this discontinuities due to geomagnetic storms was implemented.

90 As a basis for this work, this mathematical method is presented in an abbreviated way. The
 91 multiresolution analysis (AMR) is a mathematical tool used to build up wavelet functions (e.g.,
 92 Daubechies, 1992; Mallat, 1991). Then it is possible to build up wavelet functions using a pair
 93 of vectors $\{V^j, \phi^j\}$, in such a way that there are a sequence of embedded approximating spaces
 94 and the functions $V^j \subset V^{j+1}$ and ϕ_k^j form a Riesz basis for V^j , being $V^j = \text{span}\{\phi_k^j(t)\}$. In this
 95 technique, a mother-wavelet is generated from a scaling function. It obeys the following scale
 96 relation (more details in Mallat, 1991):

$$\phi(t) = 2 \sum_{k \in \mathbb{Z}} h(k) \phi(2t - k) \quad (\text{Scale relation}) \quad (7)$$

97 and $h(k)$ is the low pass-filter, also called scale filter coefficients. The family of scale relations
 98 are represented by:

$$\phi_k^j(t) = 2^{j/2} \phi(2^j t - k), \quad j, k \in \mathbb{Z} \quad (8)$$

99 They are called scale functions and in frequency domain are given by:

$$\hat{\phi}(\xi) = H(\xi/2) \hat{\phi}(\xi/2) \quad (9)$$

100 where $H(\xi) = \sum_{k \in h(k)} e^{-ik\xi}$ is a low pass filter associate to ϕ . The following relation holds:

$$V^{j+1} = V^j \oplus W^j \quad (10)$$

101 The spans W^j have the difference of information between V^j and V^{j+1} . If the ψ function form a
 102 Riesz base of W^j , it is called wavelet function:

$$\psi_k^j(t) = 2^{j/2} \psi(2^j t - k) \quad \psi(t) = 2 \sum_{k \in \mathbb{Z}} g(k) \psi(2t - k) \quad (11)$$

103 where $g(k) = (-1)^{k+1} h(-k + 1)$ is a high pass filter.

104 The wavelet and scale functions satisfy the orthogonality condition, $\langle \phi_k^j, \psi_l^j \rangle = 0$, $\langle \psi_k^j, \psi_l^m \rangle =$
 105 $\delta_{j,m} \delta_{k,l}$. The AMR tool is useful to study the function in $L^2(\mathfrak{R})$. The difference of information
 106 between V^j and V^{j+1} is given by W^j , i. e.,

$$\left(\Pi^{j+1} - \Pi^j \right) f(t) = Q^j f(t), \quad (12)$$

107 where the projections in V^j and W^j are, respectively:

$$\Pi^j f(t) = \sum_k \langle f, \phi_k^j \rangle \phi_k^j(t) \quad Q^j f(t) = \sum_k \langle f, \psi_k^j \rangle \psi_k^j(t), \quad (13)$$

108 We obtain in multi-level $j_0 < j$ the coefficients expression:

$$c_k^j = \langle f, \phi_k^j \rangle \quad d_k^j = \langle f, \psi_k^j \rangle \quad (14)$$

109 We can obtain with a change of base $\{\phi_k^{j+1}\} \leftrightarrow \{\phi_k^{j_0}\} \cup \{\psi_k^{j_0}\} \dots \cup \{\psi_k^j\}$, the equation:

$$\sum_k c_k^{j+1} \phi_k^{j+1}(t) = \sum_k c_k^{j_0} \phi_k^{j_0}(t) + \sum_{m=j_0}^j \sum_k d_k^m \psi_k^m(t) \quad (15)$$

110 In the DWT the equation (14) is manipulated jointly with to the scale relations:

$$c_k^j = \sqrt{2} \sum_m h(m-2k) c_m^{j+1} \quad d_k^j = \sqrt{2} \sum_m g(m-2k) c_m^{j+1} \quad (16)$$

111 In this work we use the Daubechies (db1) wavelet function of order 1 (Haar wavelet). In this
112 case the coefficients $h = [\frac{\sqrt{2}}{2}, \frac{\sqrt{2}}{2}]$ and consequently, $g = [-\frac{\sqrt{2}}{2}, \frac{\sqrt{2}}{2}]$.

113 The wavelet transform can be used in the analysis of non-stationary signals to rescue infor-
114 mation on the frequency or scale variations of those signals and to detect the localization of theirs
115 structures in time and/or in space. Due to the double localization property of the wavelet func-
116 tion, the wavelet transform is said to be of local type in time-frequency, with time and frequency
117 resolutions inversely proportional. As discussed by Domingues et al. (2005), one consequence
118 of the properties of the wavelet analysis is the possibility of showing that the wavelet coefficients
119 amplitude is associated with abrupt signal variations or "details" of higher frequency (see also
120 Meyer, 1990; Chui, 1992b). Selecting a wavelet function which closely matches the signal to be
121 processed is of utmost importance in wavelet applications. A tutorial on the main properties and
122 applications of the wavelet analysis can be found, for instance, in Domingues et al. (2005) and
123 Mendes et al. (2005).

124 A hard thresholding process has been applied to the wavelet coefficients for the first three
125 decomposition levels to identify the storm time in the magnetograms, as has been discussed by
126 Mendes et al. (2005). Thresholding concerns the process of setting to zero certain coefficients
127 in an effort to highlight significant information, in this case the shock-like transient phenomena
128 that appear in the main phase of the magnetic storms (see Domingues et al., 2005; Mendes et al.,
129 2005). It was found that 2^{j-1} could be used as threshold sets for the decomposition levels $(d^j)^2$,
130 because according to Meyer theorem, the multilevel threshold sets may have a multiplicity of 2
131 (Meyer, 1990).

132 In this analysis, we choose to use the Haar wavelet and the sampling rate of 1 min, as con-
133 sequence of the time resolution of the magnetic data, with the pseudo-periods of the first four
134 levels 2, 4, 8 and 16 min. The Haar wavelet is considered the most simple orthogonal analyzing
135 wavelet function. However the discrete wavelet transform (DWT) using Haar wavelet can detect
136 abrupt variations, *i. e.*, one localization feature in the physical space. The Haar wavelet has a
137 compact support in physical space and a large support in Fourier space. In other words, Haar
138 wavelet has a better localization on time than on frequency, what is expected by the Heisenberg's
139 uncertainty principle (as discussed in Daubechies, 1992).

140 4. Magnetic Data

141 In this section, we first describe the data used to study the geomagnetic variations due to the
142 tsunami-generated magnetic fields. The three tsunami's events are presented. For each event,
143 we have chosen four ground magnetic measurements. We have also selected the tide-gauge
144 measurements at or nearby the chosen magnetic stations, only for guiding purposes.

145 We selected magnetic stations belonging to the INTERMAGNET programme ([http://www.](http://www.intermagnet.org)
146 [intermagnet.org](http://www.intermagnet.org)) that were influenced or more direct affected by the tsunamis. By international
147 agreement, there are two systems that can represent the Earth's magnetic field: the XYZ and the
148 HDZ system (see Campbell, 1997, and references therein). The X, Y and Z stand for northward,
149 eastward and vertical into the Earth directions, the H, D and Z stand for horizontal component,
150 declination (angular direction of the horizontal component) and vertical (into the Earth). The H-
151 component is more affected by the solar-magnetospheric interactions, consequently, also the X-
152 and Y-component. These variations, specially those associated to the ring current, have a major
153 contribution on the magnetograms at stations located at low and mid-latitude regions. Due to
154 the Z-component be less affected than the H-component, we decided to use the Z-component to
155 detect the geomagnetic variations induced by the tsunami. Using a different technique in a work
156 with similar purpose, Manoj et al. (2011) also used the Z-component to observe the variations in
157 the Z-component provoked by the Chilean tsunami, 27 February, 2010.

158 The intensity of the geomagnetic disturbance in each day is described by indices. There are
159 different indices that can be used depending on the character and the latitude influences in focus.
160 Kp, AE and Dst and their derivations are the most used geomagnetic indices. The Kp index is
161 a number from 0 to 9 obtained as the mean value of the disturbance levels within 3-h interval
162 observed at 13 subauroral magnetic stations (see Bartels, 1957). The minutely AE index (some-
163 times 2.5 minute interval) is obtained by the H-component measured from the magnetic stations
164 located at auroral zones. The index most used in low and mid-latitudes is the Dst index. It rep-
165 represents the variations of the H-component due to changes of the ring current. The characteristic
166 signature of a magnetic storm is a depression in the horizontal component of the Earth's magnetic
167 field H and this depression is shown by the Dst index.

168 In this work, we analyzed the SYM-H index to identify periods of disturbed geomagnetic
169 field conditions. The SYM-H is essentially the same as the traditional hourly Dst index. The
170 main characteristic of the 1 minute time resolution SYM-H index is that the solar wind dynamic
171 pressure variation are more clearly seen than indices with lower time resolution. Its calculation
172 is based on magnetic data provided by 11 stations of low and medium latitude. Only six of
173 the stations are used for its calculation of each month, some stations can be replaced by others
174 depending on the data conditions.

175 We focused on the survey of geomagnetic variations induced by the tsunamis occurred at 26
176 December, 2004, 27 February, 2010 and 11 March, 2011. Related to the magnetic disturbance
177 level, these events of tsunami occurrence happened during quiet time (27 February, 2010) and
178 disturbed geomagnetic conditions (weak - 26 December, 2004, and moderate storms, 11 March,
179 2011).

180 On 26 December 2004 the Sumatra-Andaman earthquake occurred with $9.1M_w$ (M_w means
181 moment magnitude of the Richter scale) at 00 : 59 UT (Universal Time). The epicenter coordi-
182 nates are Lat. 3.4° and Long. 95.7° at 30 km depth. Tsuji et al. (2006) carried out tsunami
183 height measurements on the Andaman seacoast. They found the maximum tsunami height was
184 19.6 m at Ban Thung Dap (Lat. 9.03° and Long. 98.26°) and the second highest was 15.8 m at
185 Ban Nam Kim (Lat. 8.86° and Long. 98.28°). The tsunami not only propagated throughout the
186 Indian ocean but also into the Pacific and Atlantic oceans. Murty et al. (2005) discussed through
187 a simple analytical model that the tsunami flux from the Indian ocean into the Pacific ocean is
188 greater than the flux into the Atlantic ocean. This leakage of tsunami energy into the Pacific and
189 Atlantic oceans occurs through the gaps between Australia and Antarctica and between Africa
190 and Antarctica, respectively. The maximum tsunami amplitudes were of 0.65 m on the Pacific
191 coast and 0.3 m on the Atlantic coast as discussed by Murty et al. (2005, and references within).

192 To study the geomagnetic variations due to the Sumatra-Andaman tsunami, the magnetic
 193 stations considered were: Eyrewell (EYR), Huancayo (HUA), Learmonth (LRM) and Papeete
 194 (PPT), with the geographic and geomagnetic coordinates presented in Table 1. Figure 4 display
 195 the magnetic stations distribution and their IAGA codes. The selected tide-gauge measurements,
 196 only for guiding purposes, are located at Cocos Island (Lat. -12.12° , Long. 96.90°), Jackson
 197 Bay (Lat. -43.97° , Long. 168.62°), Nuku Hiva (Lat. -08.82° , Long. 140.20°) and Callao (Lat.
 198 -12.08° , Long. -77.13°).

Table 1: INTERMAGNET network of geomagnetic stations for the study of the Thai tsunami.

| Station | Geographic coord. | | Geomagnetic coord. | |
|---------|-------------------|-------------------|--------------------|-------------------|
| | Lat.($^\circ$) | Long.($^\circ$) | Lat.($^\circ$) | Long.($^\circ$) |
| EYR | -43.41 | 172.35 | -46.92 | -106.22 |
| HUA | -12.04 | -75.32 | -1.73 | -3.44 |
| LRM | -22.22 | 114.10 | -32.28 | -173.53 |
| PPT | -17.75 | -149.57 | -15.20 | -74.83 |

Source: <http://wdc.kugi.kyoto-u.ac.jp/igrf/gggm/index.html> (2005)

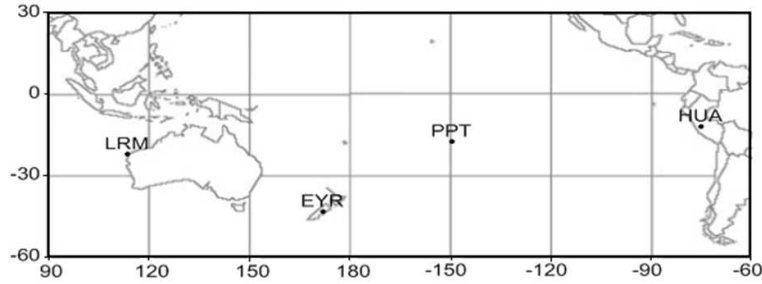


Figure 1: Geographical localization of the stations used in the study of the Sumatra-Andaman tsunami 2004

199 Near coast of the central Chile, on the 27 th of February, 2010 at 06 : 34 UT occurred
 200 an earthquake with magnitude 8.8 M_w . The epicenter was located on Lat. -36.1° and Long.
 201 -72.6° at 55 km depth. As reported by Pararas -Carayannis (2010), shortly after the earthquake,
 202 tsunami waves hit the coastal area of the Central Chile. The tsunami overtook the coastal cities
 203 as Talcahuano, Coquimbo, Antofasta and Caldera, as well as the Juan Fernández Islands. The
 204 NOAA Pacific Warning Center released a bulletin number 018 and a tsunami warning was issued
 205 at 00 : 12 UT on 28 February, 2010 for Chile, Peru, Ecuador, Colombia, Antarctica, Panama,
 206 Costa Rica, Nicaragua, Pitcairn, Honduras, El Salvador, Guatemala, French Polynesia, Mexico,
 207 Cook Islands, Kiribati, Kermadec Island, Niue, New Zealand, Tonga, American Samoa, Samoa,
 208 Jarvis Island, Wallis-Futuna, Tokelau, Fiji, Australia, Hawaii, Palmyra Island, Johnston Island,
 209 Marshall Island, Midway Island, Wake Island, Tuvalu, Vanuatu, Howland-Baker, New Cale-
 210 donea, Solomon Island, Nauru, Kosrae, Papua New Guinea, Pohnpei, Chuuk, Marcus Island,
 211 Indonesia, North Marianas, Guam, Yap, Belau, Philippines and Chinese Taipei.

212 The magnetic stations considered for this event were: Huancayo (HUA), Easter Island (IPM),
 213 Papeete (PPT) and Teoloyucan (TEO), with the geographic and geomagnetic coordinates pre-

214 sented in Table 2. Figure 4 display the magnetic stations distribution and their IAGA codes. We
 215 selected the same three stations used by Manoj et al. (2011) to study the geomagnetic contribu-
 216 tions due to the Chilean tsumani and included the station of TEO located in Mexico. In their
 217 study only the IPM station showed a periodic variation of 1 nT in the vertical component (Z)
 218 caused by the tsunami started at 11 : 35 UT, and the other two stations did not show concurrent
 219 variations.

220 The selected tide-gauge measurements are located at Callao La Punta (Lat. -12.01° and
 221 Long. -77.17°), Papeete (Lat. -17.75° and Long. -149.57°) and Acapulco (Lat. 16.83° and
 222 Long. -99.92°).

Table 2: INTERMAGNET network of geomagnetic stations for the study of the Chilean tsunami.

| Station | Geographic coord. | | Geomagnetic coord. | |
|---------|-------------------|-------------------|--------------------|-------------------|
| | Lat.($^\circ$) | Long.($^\circ$) | Lat.($^\circ$) | Long.($^\circ$) |
| HUA | -12.04 | -75.32 | -1.99 | -3.03 |
| IPM | -27.90 | -109.25 | -19.63 | -34.47 |
| PPT | -17.75 | -149.57 | -15.20 | -74.49 |
| TEO | 19.75 | -99.19 | 28.45 | -29.07 |

Source: <http://wdc.kugi.kyoto-u.ac.jp/igrf/gggm/index.html> (2010)

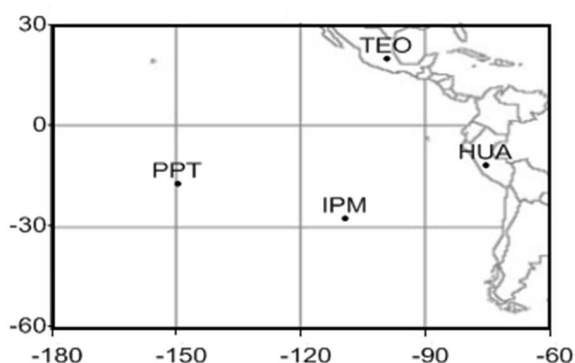


Figure 2: Geographical localization of the stations used in the study of the Chilean tsunami, 2010.

223 On 11 March, 2011, an earthquake occurred in the Japanese coast at 05 : 46 UT with $8.9 M_w$.
 224 The epicenter located at Lat. 38.3° and Long. 142.4° , near to the east coast of Honshu, at
 225 24 km depth. That earthquake induced a “major” tsunami that affected all the Japanese coast and
 226 transversed the Pacific Ocean eastward.

227 As we have done before , we also choose four stations that belong to the INTERMAGNET
 228 programme that were influenced or more directly affected by the Japanese tsunami of March 11,
 229 2011 to study the geomagnetic variations. The stations considered in this analysis were: Charters
 230 Towers (CTA), Guam (GUA), Kanoya (KNY) and Memambetsu (MMB), with geographic and
 231 geomagnetic coordinates presented in Table 3. Figure 4 display the magnetic stations distribution
 232 and their IAGA codes.

233 The selected tide-gauge measurements are located at Hanasaki (Lat. 43.28° and Long.
 234 145.57°), Tosashimizu (Lat. 32.78° and Long. 132.92°), Pago Bay (Lat. 13.43° and Long.
 235 144.80°) and Cape Ferguson (Lat. -19.28° and Long. 147.06°).

Table 3: INTERMAGNET network of geomagnetic stations for the study of the Japanese tsunami.

| Station | Geografic coord. | | Geomagnetic coord. | |
|---------|------------------|----------|--------------------|----------|
| | Lat.(°) | Long.(°) | Lat.(°) | Long.(°) |
| CTA | -20.10 | 146.30 | -27.59 | -138.58 |
| GUA | 13.28 | 144.45 | 05.18 | -144.20 |
| KNY | 31.42 | 130.88 | 22.06 | -158.71 |
| MMB | 35.44 | 144.19 | 27.09 | -146.95 |

Source: <http://wdc.kugi.kyoto-u.ac.jp/igrf/gggm/index.html> (2010)

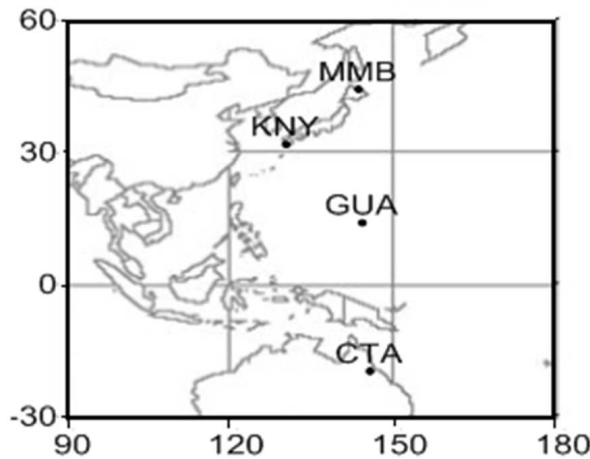


Figure 3: Geographical localization of the stations used in the study of the Japanese tsunami 2011

236 5. Results and analysis

237 Initially the wavelet treatment is done on the SYM-H Dataset, which is a processed data.
 238 According to the theory used, expected results are obtained. After that the same treatment is
 239 done directly on the magnetometer dataset for each tsunami event. The graphical results are
 240 presented and discussed validating the identifications of the tsunami occurrences (Dec. 26, 2004,
 241 Feb. 27, 2010, and Mar. 11, 2011).

242 From theory the wavelet coefficients are supposed to allow identifying the induced magnetic
 243 variations due to tsunamis, because the technique can detect physical discontinuities in the ver-
 244 tical component of the geomagnetic field. When the magnetosphere is under quiet conditions
 245 the behavior of the recorded Z-component should be much smoother than its behavior in the dis-
 246 turbed periods, making easy the identification of the variations only induced by the propagation

247 of the tsunami. Using a very localized wavelet, we will be able to detect these small geomag-
 248 netic variations. The Haar wavelet present a short compact support that provides a better local
 249 characterization of the signal and it may be the most convenient to represent times series with
 250 abrupt variations or steps.

251 5.1. Analysis on SYM-H Dataset

252 Figure 4 presents the graphical results of wavelet analysis for sample periods related to
 253 tsunami occurrences. In each part, at the top there is the SYM-H record and at the bottom
 254 respectively from the first to the fourth level of the wavelet decomposition. Based on the theory,
 255 the amplitude of the wavelet coefficients should identify the transient behavior in the dataset.

256 In the figure it is shown the discrete wavelet decomposition applied to minutely SYM-H
 257 index using Daubechies orthogonal wavelet family 1. From top to bottom each panel shows, the
 258 SYM-H and the first four levels of wavelet decomposition ($(d^j)^2$ where $j = 1, 2, 3, 4$) for the day
 259 corresponding to the tsunami of 2004 due to the Sumatra-Andaman earthquake (Figure 4a) and
 260 the day after (Figure 4b).

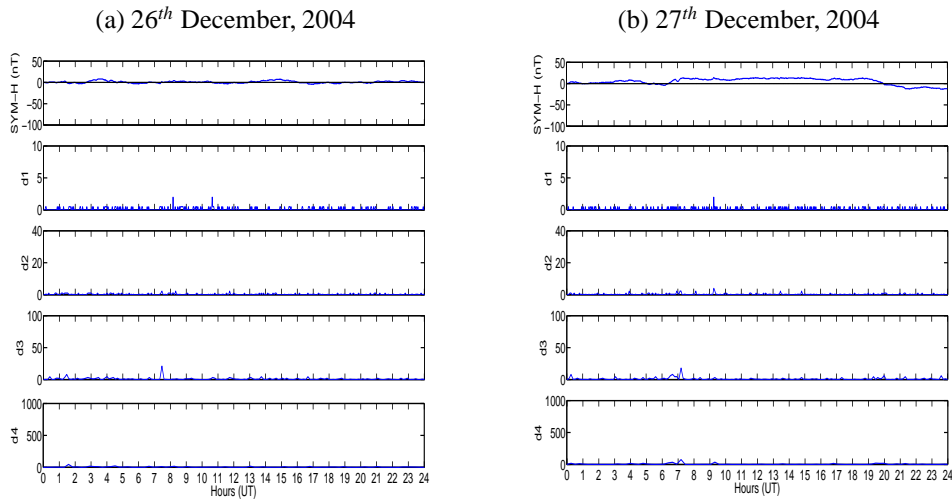


Figure 4: Graphics of SYM-H with the corresponding wavelet coefficients $(d^j)^2$ for $j = 1, 2, 3, 4$. The panel corresponds to a tsunami occurrence, (a) the arrival day and (b) the day after the Sumatra-Andaman tsunami 2004.

261 The SYM-H index analysis for the day 26 December, 2004 showed a maximum positive
 262 value of 8 nT during the period of 03 : 26 UT and 03 : 44 UT and again at 14 : 53 UT and
 263 the minimum negative value of -5 nT occurred at 17 : 00 UT (see Figure 4a). In first level of
 264 decomposition, $(d^j)^2(j = 1)$ showed two maximum of wavelets coefficients at 08 : 10 UT and at
 265 10 : 38 UT. In second level, $(d^j)^2(j = 2)$ presented the three highest values at 07 : 28 UT, 08 : 20
 266 UT and 11 : 44 UT. Only one maximum of wavelets coefficients $(d^j)^2(j = 3, 4)$ are shown in
 267 the third and fourth levels at 07 : 28 UT and 01 : 36 UT, respectively. Geomagnetic activity is
 268 classified by “size” (the amplitude of the variation in the magnetic records) and usually described
 269 by the variation of indices to distinguish between a quiet and an active day (occurrence of storm
 270 or substorm). The characteristic signature of a magnetic storm is a depression in the horizontal

271 component of the Earth's magnetic field H at middle to low latitude ground stations. The index
272 most used in low latitudes is the Dst index, similar to the SYM-H index. However SYM-H is a
273 minutely index, while Dst is a hourly index. This is the reason that the wavelet treatment were
274 done on SYM-H dataset. They represent the variations of the H component due to changes of
275 the ring current (Gonzalez et al., 1994). Following the terminology of Sugiura and Chapman
276 discussed by Gonzalez et al. (1994), the 26 December, 2004 presented a minimum Dst value of
277 -22 nT at 19 : 00 UT which corresponds to a weak geomagnetic storm. As showed on Figure 4a,
278 this day did not presented abrupt variations and consequently, in all the decompositions levels,
279 the wavelet coefficients were quite not big enough.

280 We also analyzed the SYM-H index of the day after the Sumatra-Andaman tsunami. On the
281 27 December, 2004, the SYM-H presented the maximum positive value of 14 nT at 14 : 55 nT
282 and the minimum negative value of -13 nT at 21 : 36 UT and at 23 : 44 UT. The Dst index
283 showed minimum negative value of -23 nT between 22 : 00 UT and 24 : 00 UT which
284 corresponds to a weak geomagnetic storm. Mendes et al. (2005) discussed that when the magne-
285 tosphere is under quiet conditions or the analyzed function is smooth, the wavelets coefficients
286 show very small amplitudes compare to when a geomagnetic storm is under development or
287 abrupt functions. The first and second level of decomposition showed the maximum of wavelets
288 coefficients $(d^j)^2$ ($j = 1, 2$) at 09 : 16 UT and at 09 : 16 UT, respectively. Both the third and
289 fourth level showed the maximum of wavelets coefficients $(d^j)^2$ ($j = 3, 4$) at 07 : 12 UT (see
290 Figure 4b). The wavelet coefficients also were quite not big enough.

291 As the results are referred to the analysis of a pos-processed magnetic dataset (SYM-H), the
292 wavelet coefficients were expected to be quite not big enough. The processing of the magnetic
293 records in order to create a geomagnetic index acts as a filtering process that eliminates discon-
294 tinuities. So, a result of non identifying tsunami features was already expected. In the next steps
295 we are going to deal directly with the records (magnetograms) of the selected magnetic stations.

296 5.2. 26-December-2004 tsunami event

297 In Figure 5, panels from (a) to (d) correspond to magnetic stations of LRM, EYR, PPT and
298 HUA, respectively. Each panel, from top to bottom, displays the corresponding tide gauge mea-
299 surement (sea level), the SYM-H index (both have been included for comparison purposes), the
300 corresponding magnetogram (Z component), and the wavelet signatures established by the square
301 wavelet coefficients for the four first decomposition levels, $(d^j)^2$ for $j = 1, 2, 3, 4$. The dashed
302 rectangle is related to the period of occurrence of the tsunami identified by the methodology
303 presented in this work.

304 The initial tsunami wave at the Cocos Island atoll (Australia) arrived at 03 : 17 UT and it was
305 measured with amplitude of up to 0.33 m. After the first wave arrived, following tsunami waves
306 continued for hours. As reported by the Department of Transport - Government of Western Aus-
307 tralia (<http://www.transport.wa.gov.au/imate/19383.asp>), the initial wave arrived on Exmouth
308 (Lat. -21.93° , Long. 114.13°), Australia around 06 : 30 UT. It is expected that the magnetic field
309 induced by the arrival of the tsunami will be detected at LRM around 06 : 30 UT and forward.
310 Unfortunately, only Cocos Island was the near city to the magnetic station of LRM that we were
311 able to acquire the tide gauge measurement.

312 Figure 5a shows for guiding purposes the sea level for Cocos Island. This was the near-
313 est station measurement provided by the *National Oceanic and Atmospheric Administration*
314 - NOAA (<http://wcatwc.arh.noaa.gov/about/tsunamimain.php>). We detected a small amplitude
315 coefficients at 04 : 08 UT, 17 : 00 UT and 20 : 28 UT, in the four first decomposition levels.

316 These $(d^j)^2$ ($j = 1, 2, 3, 4$) could not be explained by disturbed geomagnetic activity. Also
317 $(d^j)^2$ ($j = 1, 2, 3$) presented small amplitude coefficients at 14 : 38 UT and 22 : 40 UT.

318 In Jackson Bay, New Zealand, the initial wave arrived at 15 : 10 UT with amplitudes up to
319 0.65 m. In order to verify the transients due to the tsunami we used the EYR magnetogram data
320 (see Figure 5b). For $(d^j)^2$ ($j = 1$), the highest wavelet amplitudes were detected at 03 : 58 UT,
321 05 : 08 UT, 18 : 00 UT, 20 : 36 UT and 21 : 22 UT. We are only detecting the highest amplitudes
322 that do not correspond to the wavelet coefficients signature detected by the previously SYM-H
323 index analysis. The $(d^j)^2$ ($j = 2$) presented the highest amplitude coefficients at 03 : 58 UT
324 and 19 : 52 UT. The maximum amplitude $(d^j)^2$ ($j = 3$) value occurred at 22 : 40 UT. For $(d^j)^2$
325 ($j = 4$), the highest wavelet amplitudes occurred at 04 : 16 UT, 05 : 04 UT, 17 : 04 UT, 20 : 00
326 UT, 21 : 36 UT and 23 : 12 UT.

327 Figure 5c shows the wavelet decompositions for the PPT, French Polynesia. As reported
328 by NOAA, the initial wave arrival could not be determined exactly. For guiding purposes, we
329 presented the sea level variations at Nuku Hiva, French Polynesia. At all the four decomposition
330 levels, we detected perceptible $(d^j)^2$ ($j = 1, 2, 3, 4$) amplitudes between 15 : 00 UT and 20 : 00
331 UT that might be due to the tsunami propagation.

332 On 27 December, 2004, the tsunami waves that propagated throughout the Pacific Ocean
333 arrived at the coast of Peru (see Figure 5c). At Callao, Peru, the initial tsunami wave arrived at
334 05 : 20 UT with maximum wave height of 0.65 m. The $(d^j)^2$ for $j = 1, 2, 3, 4$ decomposition
335 levels showed what might be tsunami transients between 13 : 00 UT and 19 : 00 UT.

336 Thus from the methodology applied, the transients in the magnetogram, that are not related
337 to geomagnetic storms, are identified by the wavelet coefficients. Those transients are not related
338 to the common geomagnetic disturbance causes, but some remarkable coefficients are related to
339 the ocean stream. The dashed rectangles in each panel of the figure indicate the identification of
340 the transients associated to the tsunami magnetic effects.

341 5.3. 27-February-2010 tsunami event

342 In the region of Callao La Punta, Peru, the observed and computed tsunami time arrival were
343 coincident, both at 10 : 34 UT with amplitude of up to 0.69 m. We used the sea level measured
344 at this region as guiding line to the arrival tsunami at HUA and IPM (see Fig 6a-b). Fig 6 is very
345 similar to Figure 5, also shows the wavelet signatures for the four first decomposition levels ($(d^j)^2$
346 where $j = 1, 2, 3, 4$). Panels from (a) to (d) correspond to magnetic stations of HUA, IPM, PPT
347 and TEO, respectively. In each panel, from top to bottom are displayed the corresponding tide
348 gauge measurement, the SYM-H index, the corresponding magnetogram (Z component), and
349 the $(d^j)^2$ for $j = 1, 2, 3, 4$ decomposition levels. On geomagnetic conditions, the 27 February,
350 2010 corresponded to a very quiet day. The Dst index presented the minimum of -2 nT and
351 the maximum of 4 nT with very smooth variations. The SYM-H also presented very smooth
352 variations with the minimum of -9 nT and the maximum of 5 nT.

353 In Fig 6a, the $(d^j)^2$ for $j = 1, 2, 3, 4$ decomposition levels presented quite similar behaviors.
354 Also, they showed a main structure of coefficients which are preceded and followed by a se-
355 quence of small structures after 11 : 00 UT. The highest wavelet coefficient amplitudes occurred
356 at 11 : 26 UT, 15 : 26 UT, between 16 : 42 UT and 18 : 12 UT, 19 : 48 UT and between 21 : 00
357 UT and 21 : 48 UT.

358 The NOAA Pacific Warning Center predicted the tsunami time arrival at 12 : 05 UT for
359 the Easter Island, IPM. In Fig 6b, the first decomposition level presented a main structure of
360 coefficients between 11 : 58 UT and 13 : 24 UT and a secondary pike at 15 : 36 UT, also

361 presented a sequence of small structures between 16 : 54 UT and 24 : 00 UT. $(d^j)^2(j = 2)$
362 showed the highest coefficients at 12 : 28 UT and 12 : 40 UT and $(d^j)^2(j = 3)$ at 12 : 00 UT.
363 $(d^j)^2(j = 2, 3)$ presented less structured features than $(d^j)^2(j = 1, 4)$. In $(d^j)^2(j = 4)$ was possible
364 to notice two peaks, one at 12 : 00 UT and the other at 12 : 32 UT, followed by a main structure
365 of coefficients between 17 : 04 UT and 19 : 28 UT and a secondary structure between 20 : 48
366 UT and 21 : 06 UT.

367 Fortunately, for PPT, we were able to get the tide gauge measurements at the same location
368 (see Fig 6c). The observed tsunami initial arrival time was at 17 : 33 UT and the computed time
369 was at 17 : 47 UT with amplitude up to 0.22 m. The $(d^j)^2(j = 1, 2, 3, 4)$ presented surprisingly
370 similar wavelet signatures. In Fig 6c, the main wavelet coefficient structures are restricted be-
371 tween 15 : 36 UT and 21 : 52 UT. The tsunami-induced electromagnetic field effects could be
372 detected about two hours in advance.

373 We also selected a further located station TEO in Mexico with the purpose of analyzing if
374 we could detect any geomagnetic tsunami effects. For guiding purposes, we used the tide gauge
375 measurements at Acapulco. The observed tsunami initial arrival time was at 15 : 47 UT with
376 amplitude up to 0.66 m. In Fig 6d, the $(d^j)^2(j = 1)$ showed an even more structured signature than
377 $(d^j)^2(j = 2, 3, 4)$. The highest wavelet amplitudes coefficients for $(d^j)^2(j = 1)$ was at 14 : 26 UT,
378 16 : 34 UT, 18 : 16 UT, 19 : 40 UT, 20 : 34 UT and 21 : 24 UT. The $(d^j)^2(j = 2, 3, 4)$ presented
379 a quite similar signature but less structured features than $(d^j)^2(j = 1)$. It was possible notice the
380 presence of highest wavelet amplitudes coefficients after 12 : 52 UT for $(d^j)^2(j = 2, 3, 4)$ that
381 could be related to the tsunami effects.

382 5.4. 11-March-2011 tsunami event

383 On 11 March, 2011, occurred a geomagnetic disturbance which corresponded to a moderate
384 storm with minimum Dst = -82 nT at 06 : 00 UT and a second energy injection at 18 : 00 UT
385 with minimum Dst = -67 nT at 22 : 00 UT. So, the abrupt variations of the vertical component
386 of the geomagnetic field due to the development of this moderate storm will be more emphasized
387 by the highest amplitudes of the wavelet coefficients.

388 In Figure 7, the highest coefficients of all the four levels detected in the SYM-H are restricted
389 to the development of the storm following the second energy injection at 18 : 00 UT, specially
390 during the main phase of the geomagnetic storm between 18 : 00 UT and 24 : 00 UT presented
391 the highest wavelet coefficients amplitudes which was usually observed by Domingues et al.
392 (2005). All the decomposition levels show quite similar behaviors, showing the highest wavelet
393 coefficients $(d^j)^2(j = 1, 2, 3, 4)$ soon after the recovery time of the first storm and associated with
394 the fluctuations of the SYM-H index as the second magnetic storm came to the minimum value.

395 Figure 8 is very similar to Figure 5 and Fig 6. It also shows the wavelet signatures for the
396 four first decomposition levels, $(d^j)^2$ for $j = 1, 2, 3, 4$. Panels from (a) to (d) correspond to
397 magnetic stations of HUA, IPM, PPT and TEO, respectively. In each panel, from top to bottom
398 are displayed the corresponding tide gauge measurement, the SYM-H index (both have been
399 included for comparison purposes only), the corresponding magnetogram (Z component), and
400 the $(d^j)^2$ for $j = 1, 2, 3, 4$ decomposition levels. We decided to exclude the period between
401 18 : 00 UT and 24 : 00 UT, as shown in Figure 7, because the wavelet coefficients in this period
402 were related to the abrupt variations caused by the second energy injection in the geomagnetic
403 storm.

404 In the city of Hanasaki, near to the magnetic station of MMB, the initial phase of the tsunami
405 started at 06 : 38 UT and reached the maximum height (0.74 m) at 06 : 57 UT. We used the

406 tide gauge measurements at Hanasaki in Figure 8a for guiding purposes. The $(d^j)^2(j = 1, 2, 3, 4)$
407 showed a very structured signature. Also, $(d^j)^2(j = 1, 2, 3)$ showed a main structure of wavelet
408 coefficients that could be noticed between 06 : 00 UT and 08 : 00 UT, a secondary structure
409 between 10 : 00 UT and 11 : 20 UT and a smaller structure between 16 : 00 UT and 18 : 00 UT.
410 The $(d^j)^2(j = 4)$ showed less structured features than $(d^j)^2(j = 1, 2, 3)$ and presented the highest
411 amplitudes at 07 : 12 UT, 10 : 56 UT and 17 : 04 UT. We can observe at the first decomposition
412 level, a presence of wavelet coefficients at 06 : 26 UT which corresponds to the tsunami initial
413 phase. At 06 : 57 UT, when tsunami reached the maximum height, we also notice the presence
414 of an increase in the coefficient amplitudes with the maximum at 07 : 04 UT higher than the
415 coefficient at the initial phase. Meanwhile, $(d^j)^2(j = 2, 3, 4)$ associated to the tsunami presented
416 more spread on time and did not present any remarkable amplitudes corresponding to its initial
417 phase and maximum height.

418 Near to the KNY station, in the city of Tosashimizu, the tsunami started at 07 : 51 UT and the
419 maximum height (1.28m) was measured at 16 : 58 UT (see Figure 8b). The wavelet signatures of
420 $(d^j)^2(j = 1, 2, 3, 4)$ show very similar structures. The $(d^j)^2(j = 1, 2)$ showed the highest wavelet
421 amplitudes around 06 : 04 UT and 17 : 02 UT. And the $(d^j)^2(j = 3, 4)$ showed the highest
422 wavelet amplitudes around 06 : 08 UT, 06 : 40 UT, 07 : 44 UT, 10 : 40 UT, 16 : 48 UT and
423 17 : 52 UT. This Japanese magnetic station showed surprisingly similar signatures compared to
424 Figure 8a. We also observe, in third and fourth decomposition levels, the presence of wavelet
425 coefficients $(d^j)^2(j = 3, 4)$ around the tsunami initial phase and maximum height.

426 In Figure 8c, the observed time of the tsunami's arrival at Pago Bay, Guam around 09 : 16 UT.
427 The tsunami maximum height occurred at 09 : 58 UT and its amplitude was up to 0.54 m. GUA
428 magnetic station did not show any coefficient $(d^j)^2(j = 1, 2, 3, 4)$ that represented significant
429 contribution due to the tsunami. At the same time, we observe the presence of small coefficients
430 $(d^j)^2(j = 1, 2, 3, 4)$ but still noticeable between 10 : 40 UT and 11 : 28 UT.

431 The predicted time of the tsunami's arrival by NOAA at Cairns (Lat. -16.57° and Long.
432 145.75°), Australia, would be at 15 : 35 UT. Unfortunately, at Cape Ferguson, it was not possible
433 to determine the exactly tsunami time arrival (see Figure 8d). The tide gauge measurements
434 registered the tsunami maximum height at 21 : 00 UT with amplitudes up to 0.11 m. The CTA
435 magnetic station did not show any remarkable wavelet coefficient amplitudes $(d^j)^2(j = 1, 2, 3, 4)$
436 due to the tsunami.

437 In summary, the wavelet coefficient of the first three levels of decomposition showed a good
438 time localization of the initial phase and the maximum height of the Japanese tsunami at 11th of
439 March, 2011 and they, also, were locally associated with the geomagnetic variations present in
440 the signal due to the secondary magnetic fields induced by the movement of electrically conduct-
441 ing sea-water through the geomagnetic field. The red vertical lines in each panel of the figure
442 indicate the identification of the first transient associated to the tsunami magnetic effects.

443 Thus from the several events analyzed the wavelet method for identification of the tsunami
444 magnetic effects could be validated, characterizing an useful tool for this kind of study in order
445 to deal with very weak but significant amplitude of wavelet coefficients.

446 6. Conclusions

447 Dealing with the geomagnetic data analyzed by discrete wavelet transform using Haar wavelet,
448 this work aimed to implement a methodology for the direct analysis of magnetograms and to ver-
449 ify the occurrence of tsunami effects on Z-component of the geomagnetic field. The carried out
450 analysis can be summarized as follows:

- 451 • The wavelet technique is useful to “zoom in” the localized behavior of the geomagnetic
452 variations induced by the movement of electrically conducting sea-water through the ge-
453 omagnetic field; *i. e.*, the identification of magnetic transients related to the tsunamis. As
454 well, from the analysis of the magnetogram data, it was able to localize the initial phase
455 and maximum height of the tsunamis in some cases.
- 456 • The discrete wavelet transform (Daubechies - db1) provides a very good local characteri-
457 zation of the signal and may be the most convenient to represent times series with abrupt
458 variations or steps, *i. e.*, very small and localized variations as the discontinuities in the
459 Z-component due to tsunamis.
- 460 • The discrete wavelet transform is an alternative way to analyze the global influence of the
461 tsunamis on the geomagnetic field and it could be used as a sophisticated tool to predict
462 the tsunami arrival, as an example of the Chilean tsunami, the DWT detected transients
463 about two hours in advance at Papeete.

464 The results obtained are encouraging even with a few of events. The present study dealt
465 with only three tsunami events and few magnetic stations. A future study using more events and
466 more stations should be very good in order to do a more complete analysis of features. The first
467 interpretation of the results suggests that discrete wavelet transform can be used to characterize
468 the tsumanis effects on the geomagnetic field.

469 7. Acknowledgments

470 V. Klausner wishes to thanks CAPES for the financial support of her PhD. A. R. R. P. thanks
471 CNPq for a research fellowship. This work was supported by CNPq (grants 309017/2007-6,
472 486165/2006-0, 308680/2007-3, 478707/2003, 477819/2003-6, 382465/01-6), FAPESP (grants
473 2007/07723-7) and CAPES (grants 86/2010-29). Also, the authors would like to thank the IN-
474 TERMAGNET programme for the datasets used in this work.

475 References

- 476 Bartels, J., 1957. The technique of scaling indices k and q of geomagnetic activity. *Annals of the International Geophys-*
477 *ical Year* (4), pp. 215–226.
- 478 Campbell, W. H., 1997. *Introduction to Geomagnetic Fields*. Cambridge University Press, New York.
- 479 Chui, C., 1992a. *An introduction to wavelets*. Academic Press, San Diego, CA 1.
- 480 Chui, C., 1992b. *Wavelets: A tutorial in theory and applications*. Academic Press, San Diego, CA 2.
- 481 Chui, C., 1994. *Wavelets theory, algorithms and applications*. Academic Press, San Diego, CA 5.
- 482 Cueto, M., McKnight, D., Herraiz, M., 2003. Daily geomagnetic variations on the Iberian peninsula. *Geophysical Journal*
483 *International* 152 (1), pp. 113–123.
- 484 Daubechies, I., 1992. Ten lectures on wavelets. In: *CBMSNSF Regional Conference Series in Applied Mathematics*,
485 *SIAM*, Philadelphia, PA. Vol. 61.
- 486 Domingues, M. O., Mendes, O. J., Mendes da Costa, A., 2005. Wavelet techniques in atmospheric sciences. *Advances*
487 *in Space Research* 35 (5), pp. 831–842.
- 488 Gonzalez, W., Joselyn, J., Kamide, Y., Kroehl, H., Rostoker, G., Tsurutani, B. T., Vasyliunas, V., 1994. What is a
489 geomagnetic storm? *Journal of Geophysical Research* 99 (A4), pp. 5771–5792.
- 490 Larsen, J., Cox, C., 1966. Lunar and solar daily variation in the magnetotelluric field beneath the ocean. *Journal of*
491 *Geophysical Research* 71, pp. 4441.
- 492 Longuet-Higgins, M. S., Stern, M. E., Stommel, H., 1954. The electrical field induced by ocean currents and waves,
493 with applications to the method of towed electrodes. *Papers in Physical Oceanography and Meteorology*, WHOI and
494 MIT, Cambridge and Woods Hole, pp. 37.

- 495 Mallat, S., 1991. Multiresolution approximations and wavelets orthonormal bases. *Transactions of American Mathematical Society* 315, pp. 334–351.
- 496
- 497 Manoj, C., Kuvshinov, A., Maus, S., Luhr, H., 2006. Ocean circulation generated magnetic signals. *Earth, Planets and Space* 58, pp. 429-437.
- 498
- 499 Manoj, C., Maus, S., Chulliat, A., 2011. Observation of Magnetic Fields Generated by Tsunamis. *EOS, Transactions American Geophysical Union* 92 (2), pp. 13.
- 500
- 501 Mendes, O. J., Domingues, M. O., Mendes da Costa, A., 2005. Wavelet analysis applied to magnetograms. *Journal of Atmospheric and Solar-Terrestrial Physics* 67, pp. 1827–1836.
- 502
- 503 Mendes da Costa, A., Domingues, M. O., Mendes, O., Brum, C. G. M., 2011. Interplanetary medium condition effects in the south atlantic magnetic anomaly: A case study. *Journal of Atmospheric and Solar-Terrestrial Physics*.
- 504
- 505 Meyer, Y., 1990. *Ondelettes et Operateurs*. Hermann, Paris.
- 506
- 507 Morlet, J., 1983. Sampling theory and wave propagation. In: Chen, C. (Ed.), *Acoustic Signal/Image Processing and Recognition*, in NATO ASI. Springer-Verlag, New York., Vol. 1. pp. 233–261.
- 508
- 509 Murty, T. S., Nirupama, N., Rao, A. D., 2005. Leakage of the Indian Ocean tsunami energy into the Atlantic and Pacific Ocean. *CSEG Recorder*, pp. 33–36.
- 510
- 511 Parkinson, W. D., 1983. *Introduction to geomagnetism*. Scottish Academy Press, Edinburg and London.
- 512
- 513 Pararas -Carayannis, G., 2010. The earthquake and tsunami of 27 February 2010 in Chile - Evaluation of source mechanism and of near and far-field tsunami effects. *Science of tsunami hazards* 29 (2), pp. 96–126.
- 514
- 515 Podney, W., 1975. Electromagnetic Fields Generated by Ocean Waves. *Journal of Geophysical Research* 80 (21), pp. 2977–2990.
- 516
- 517 Tyler, R. H., Oberhuber, J. M., Sanford, T. B., 1999. The potential for using ocean generated electromagnetic fields to remotely sense ocean variability. *Physics and Chemistry of the Earth, Part A: Solid Earth and Geodesy* 24 (4), pp. 429–432.
- 518
- 519 Tyler, R. H., Maus, S., Luhr, H., 2003. Satellite observations of magnetic fields due to ocean tidal flow. *Science* 299, pp. 239–241.
- 520
- 521 Tsuji, Y., Namegaya, Y., Matsumoto, Y., Iwasaki, S.I., Kanbua, W., Sriwichai, M., Meesuk, M., 2006. The 2004 Indian tsunami in Thailand: Surveyed runup heights and tide gauge records. *Earth, Planets and Space* 58, pp. 223–232.

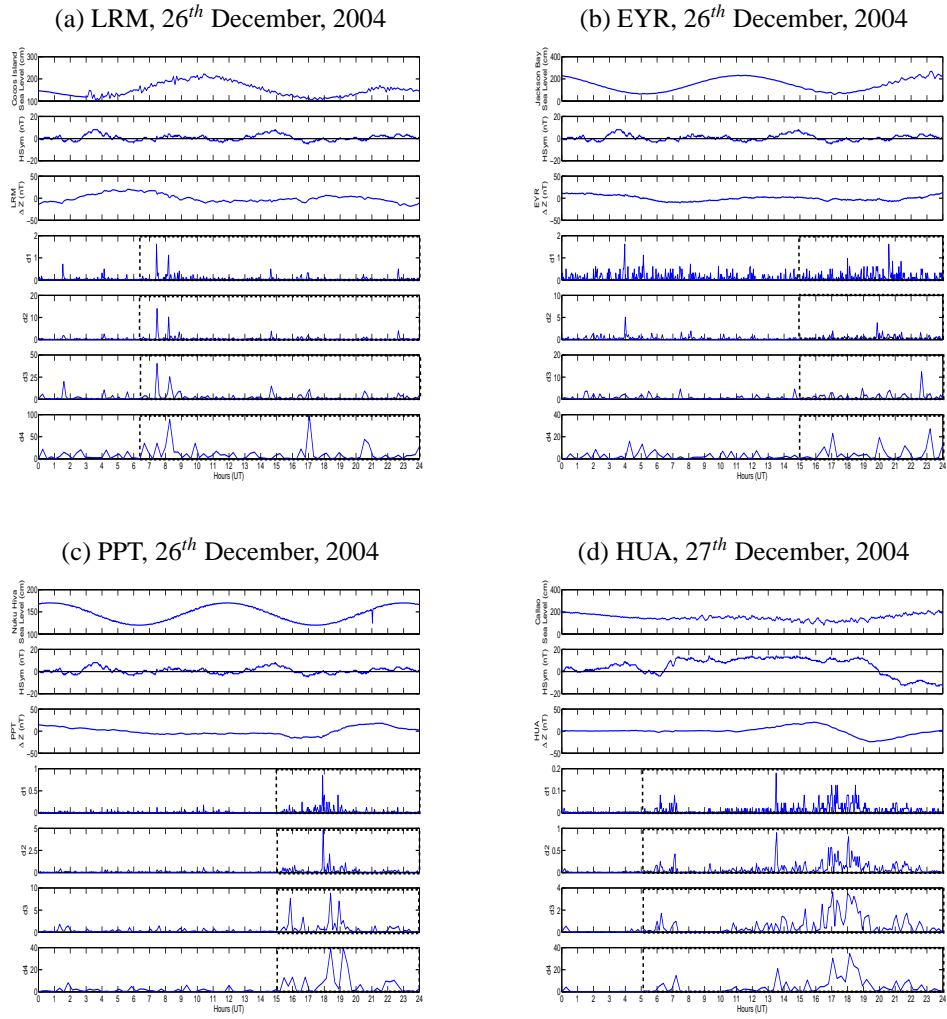


Figure 5: Magnetograms and the wavelet coefficients $(d^j)^2$ for $j = 1, 2, 3, 4$ (a-d) for LRM, EYR, PPT and HUA, respectively.

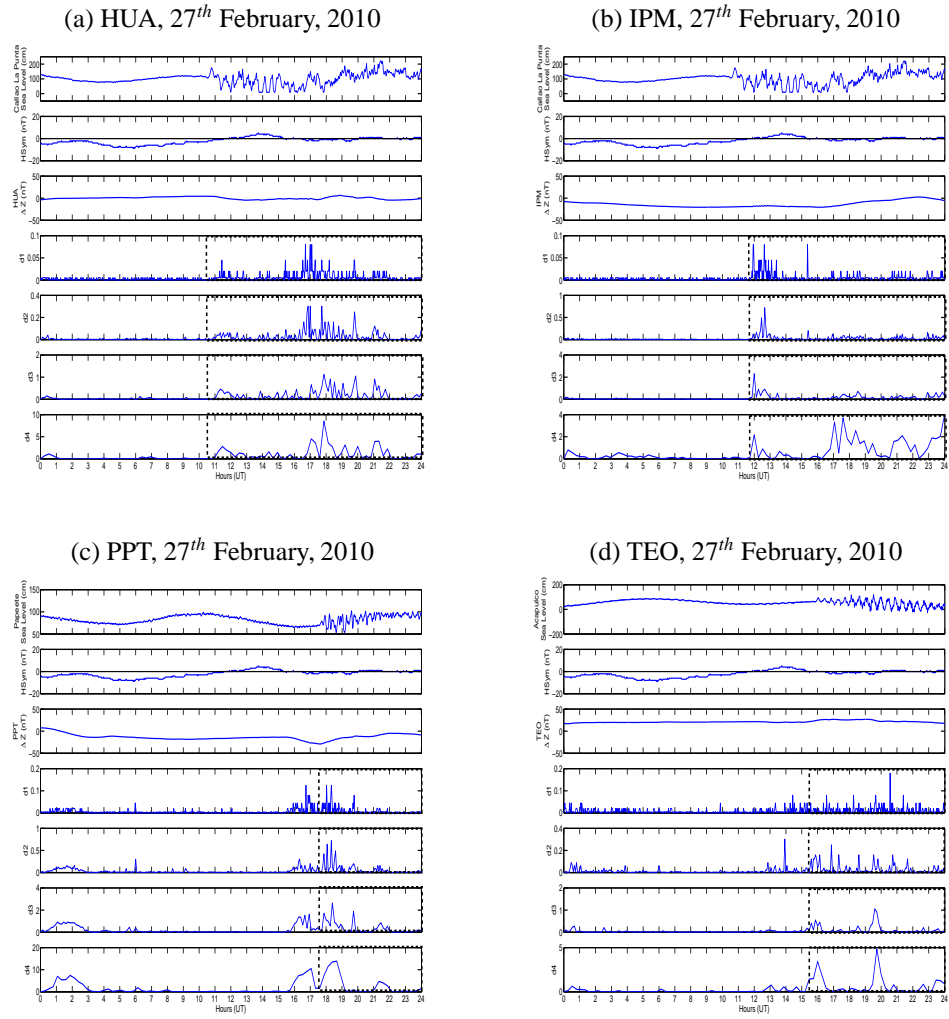


Figure 6: Magnetograms and the wavelet coefficients $(d^j)^2$ for $j = 1, 2, 3, 4$ (a-d) for HUA, IPM, PPT and TEO, respectively.

11th March, 2011

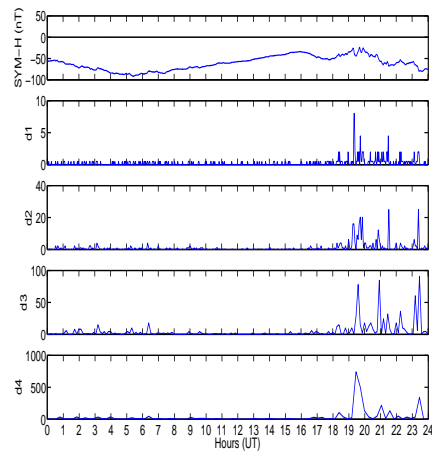


Figure 7: Graphics of SYM-H with the corresponding wavelet coefficients $(d^j)^2$ for $j = 1, 2, 3, 4$. The panel corresponds to a Japanese tsunami occurrence at 2011.

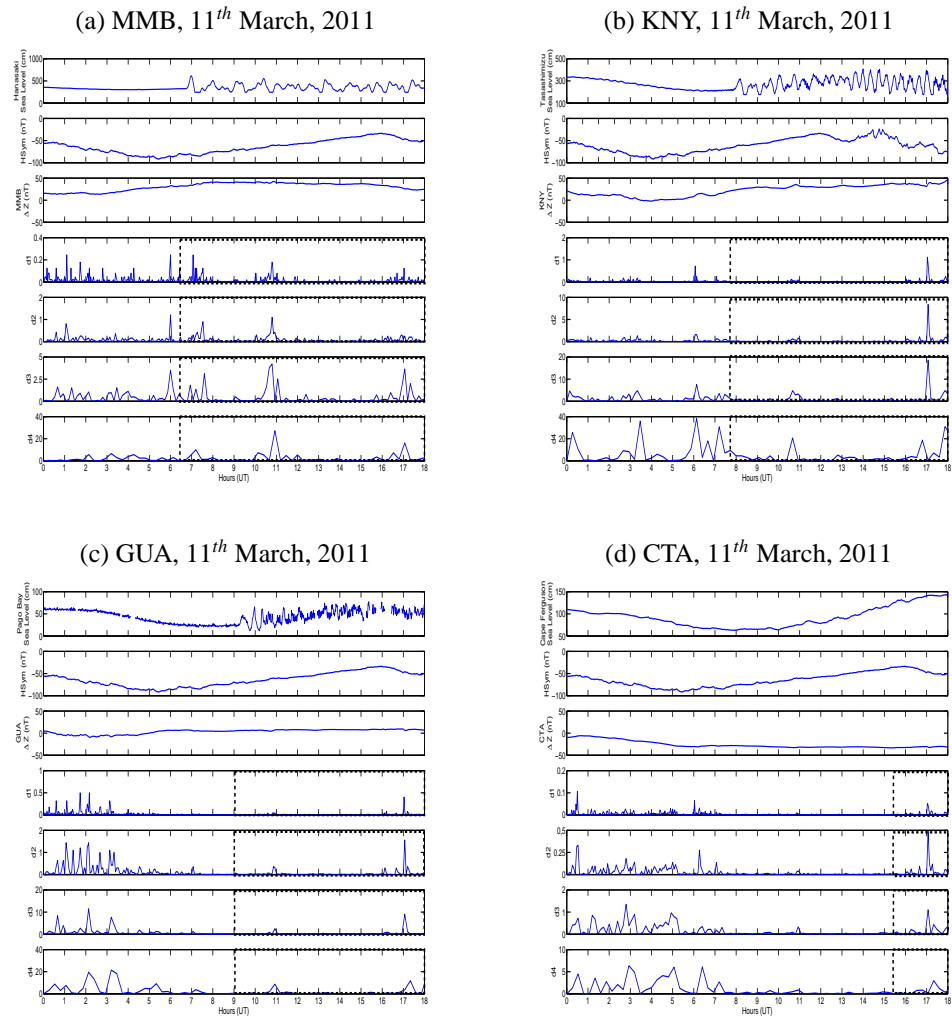


Figure 8: Magnetograms and the wavelet coefficients $(d^j)^2$ for $j = 1, 2, 3, 4$ (a-d) for MMB, KNY, GUA and CTA, respectively.